A comparative evaluation of differently synthesized high surface area carbons for Li-ion hybrid electrochemical supercapacitor application: Pore size distribution holds the key

Anil Suryawanshi [a,b], Mandakini Biswal [a], Dattakumar Mhamane [a], Prasad Yadav [a], Abhik Banerjee [a], Poonam Yadav [a], Shankar Patil [b], Vanchiappan Aravindan [c,], Srinivasan Madhavi [c,d,]* and Satishchandra Ogale [a,]**

[a] Centre of Excellence in Solar Energy, National Chemical Laboratory (CSIR-NCL), Dr Homi Bhabha Road, Pune 411008,

[b] Department of Physics, Savitribai Phule Pune University, Pune 411008, India

[c] Energy Research Institute @ NTU (ERI@N), Nanyang Technological University, Research Techno Plaza, 50 Nanyang Drive, Singapore 637553.

[d] School of Materials Science and Engineering, Nanyang Technological University, Singapore 639798.

* Corresponding Author: Dr. Satishchandra Ogale

Centre of Excellence in Solar Energy, National Chemical Laboratory (CSIR-NCL), Dr. Homi Bhabha Road, Pune, 411008. India. Phone: +912025902260, +919822628242, Fax: +912025902636.

E-mail address: satishogale@gmail.com (S.Ogale), aravind_van@yahoo.com (V. Aravindan), Madhavi@ntu.edu.sg (S. Madhavi)

Abstract

We report a comparative evaluation of carbonaceous cathodes synthesized by different protocols in the context of Li-ion hybrid electrochemical supercapacitors (Li-HEC) application. The four cathode materials compared include hierarchically perforated graphene (HPGN), Polymer (Poly (4-styrene sulfonic acid-co-maleic acid) sodium salt) derived Graphene (PDG), dead neem leaves derived carbon (LDC) and commercial activated carbon (CAC). All these carbons exhibit high specific surface area with excellent porosity. In the single electrode configuration (*vs.* Li), HPGN shows maximum specific capacitance of ~155 F g^{-1} with good cycleability over 1000 cycles (99.5% retention). On the other hand, there is no obvious distinctive difference between the specific capacitance values for the rest of the carbonaceous materials tested. The Li-HEC is constructed with spinel phase $Li_4Ti_5O_{12}$ anode and carbonaceous materials described above as cathode in a non-aqueous medium. Amongst the various cases the Li-HEC with HPGN delivered maximum energy and corresponding power density of 65 Wh kg^{-1} and 0.5 kW kg^{-1}, respectively with excellent cycleability as compared to the rest of the materials, tested in the same configuration under the same testing conditions.

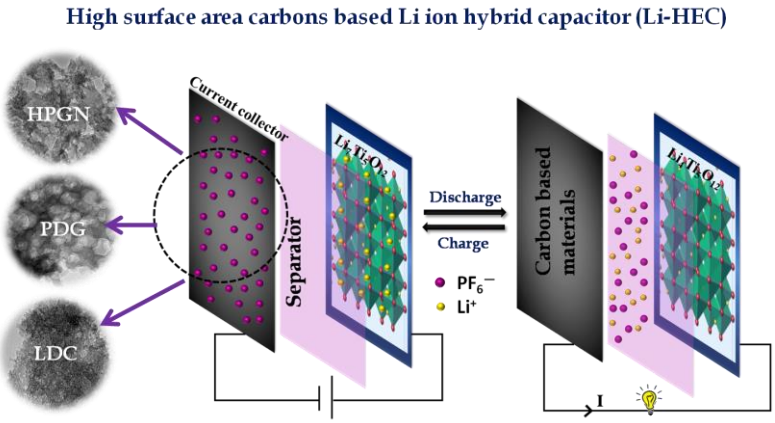

Keywords: Porous Carbon; Li-ion capacitor; Cathode; Energy density; Pore Size.

1. Introduction

As of today, in the frame of energy storage, the major scientific efforts have been expended in the area of Electrochemical Double Layer Capacitors (EDLC) [1-3]. However, the most important question of limited energy density has remained unsolved for prospective advanced applications such as hybrid electric vehicles (HEV) and electric vehicles (EV) [4]. In the conventional EDLC configuration, carbonaceous materials such as activated carbon (AC) [5-7], carbon nanotubes (CNT)[3,8] and graphene nanosheets (GNS) [9,10] have dominated as electro-active materials irrespective of the electrolyte medium owing to their high specific surface area, excellent chemical stability in electrolyte solutions with different pH levels, low cost and amphoteric nature which allows rich electrochemical properties from donor to acceptor state with wide operating temperatures [5]. Although, EDLC delivers excellent power density it fails to display practical energy density beyond ~10 Wh kg^{-1} [11]. Therefore, EDLC alone is not truly capable of powering HEV and EV [12]. On the other hand, Li-ion batteries (LIB) offer high energy density, but lack the desired power density to drive such vehicles [1, 4, 13]. In this scenario, it is very challenging to overcome the limitations of individual systems like EDLC and LIB. One of the best solutions to solve this problem is to integrate both systems to obtain higher energy and power densities and such a configuration is called Li-ion hybrid electrochemical capacitor (Li-HEC). The Li-HEC is expected to bridge the huge gap between EDLC and LIB. Similar to EDLC, utilization of aqueous medium is not appreciated due to the water splitting issues (~1.23 V). Therefore, exploitation of non-aqueous solutions is anticipated and such concept is originally proposed by Amatucci *et al.* [14, 15]. Generally, Li-HEC consists of Li-insertion type electrode (battery component) coupled with high surface area carbonaceous materials preferably AC as counter electrode (supercapacitor component) in Li-ion conducting

non-aqueous electrolytes. There are numerous Li-insertion type materials such as pre-lithiated graphite, $Li_4Ti_5O_{12}$ [11, 12, 16-19], $LiCrTiO_4$ [20,21], MnO_2 [22, 23], TiO_2-B [24, 25], β-FeOOH [26], TiP_2O_7 [27], $LiTi_2(PO_4)_3$[28], Li_2MnSiO_4 [29], Li_2FeSiO_4 [30], $LiFePO_4$ [31], $LiCoPO_4$ [32], $LiMn_2O_4$, $LiNi_{0.5}Mn_{1.5}O_4$ [33], V_2O_5 [34], Li_2CoPO_4F [35], which have been explored along with carbonaceous counter electrodes in non-aqueous medium. Among them, spinel phase $Li_4Ti_5O_{12}$ is found to be appealing due to its salient features like no volume variation during Li-insertion/extraction (Zero strain host), appreciable theoretical capacity (~175 mAh g^{-1}) with high reversibility, thermodynamically flat operating potential (~1.55 V *vs.* Li), easy synthesis and eco-friendliness [36]. Although pre-lithiated graphite anode delivers very high energy density in Li-HEC configuration, the tedious pre-lithiation and solid electrolyte interface during such lithiation process hinders the mass production [12, 18]. Hence, much attention is paid to develop insertion type transition metal oxides for Li-HEC applications. Compared to the Li-insertion type materials, there is not much work reported on the development of carbonaceous electrodes, except AC. However, the energy density is limited to ~14 Wh kg^{-1} when coupled with $Li_4Ti_5O_{12}$ anode, in spite of its high specific surface area. This may be due to the poor conductivity (poor degree of graphitization) and random pore structure. Currently, great attention is being paid to the development of high surface area carbonaceous materials with porous nature. Among the carbonaceous materials, graphene is found noteworthy due to its high specific capacitance with good cycleability in EDLC configuration, high surface area (2630 m^2 g^{-1}), excellent electrical conductivity and good chemical and thermal stabilities [37]. Recently, Stoller *et al*. [38] first reported the performance of KOH treated microwave exfoliated graphene oxide (a-MEGO) with $Li_4Ti_5O_{12}$ anode in Li-HEC assembly with a delivered energy density of 40.8 Wh kg^{-1}. Recently, tailoring of graphene into 3D form, functionalized graphene, nano-perforated graphene, porous

graphene derived by pyrolysis of polymer and porous carbon derived from dead leaves have been explored as outstanding electrode material for EDLC [39-41]. Owing to the extraordinary performance in EDLC configuration and easy synthesis protocol, we set out to examine these forms for the construction of high energy density Li-HEC. We optimized the mass loading for constructing Li-HEC based on the electrochemical performance of HPGN, PDG, LDC and commercially available activated carbon (CAC) in a single electrode configuration *vs.* Li. The detailed structural and electrochemical performances were carried out along with the spinel phase $Li_4Ti_5O_{12}$ anode in Li-HEC configuration and are described in detail.

In this work we demonstrate that amongst the four materials under study viz. three novel carbon nanoforms (HPGN, PDC and LDC) and one conventional form CAC, the HPGN material performed well in terms of impressive electrochemical properties in Li-HEC. We highlight the importance of HPGN electrode in perspective energy storage context. For example, in the single electrode configuration (*vs.* Li), HPGN displayed high specific capacitance of ~155 F g^{-1} with 99.5% retention in the initial capacitance over 1000 cycles with maximum energy density and corresponding power density of 65 Wh kg^{-1} and 0.5 kW kg^{-1}, respectively. The other three materials PDC, LDC and CAC showed limited performance with specific capacitance values of 86, 74 and 72 F g^{-1}, respectively. The observed results for HPGN are almost double as compared to the other electrodes. The reasons for the best performance of HPGN are discussed.

2. Experimental

2.1 Materials

Spinel phase $Li_4Ti_5O_{12}$ nanaoparticles (particle size < 100 nm with a surface area of 32.6 m^2 g^{-1}) and CAC (surface area of 880 m^2 g^{-1}) were procured from Sigma-Aldrich, USA and Norit, The Netherlands, respectively and used without any further treatment.

2.2 Synthesis of hierarchically nano-perforated graphene (HPGN)

Initially graphite oxide (GO) was prepared by harsh oxidation of graphite powder by using the modified Hummer's method. The step by step synthetic process of GO and its purification is discussed in our previous report [42]. Briefly, 100 mg of GO was homogeneously dispersed in 100 ml de-ionized (DI) water by means of strong sonication (~1 h). To the above homogeneous brown dispersion of GO 100 mL of Ludox (colloidal solution of 12 nm silica nanoparticles) solution was added. The above mixture was stirred (24 h) and finally the product was separated by centrifugation. The attached SiO_2 particles were removed by adding sufficient amount of HF. The product was then washed several times with DI water and finally re-dispersed in 100 ml DI water and reduced using hydrazine hydrate to yield HPGN.

2.3 Synthesis of Polymer derived graphene (PDG)

3D Hexaporous graphene was synthesized according to the process proposed by Yadav *et al.* [40]. In a typical procedure Poly (4-styrene sulfonic acid-co-maleic acid) sodium salt was pyrolyzed at 1000 °C for 4 h in Ar atmosphere. The obtained black powder was washed several times with DI water to remove associated inorganic impurities and finally the product was dried in vacuum oven to obtain polymer derived graphene (PDG).

2.4 Porous carbon derived from dead leaves (LDC)

The details of the process used to obtain this form of carbon and the choice of precursor are described in our recent publication [41]. Briefly; dead leaves of Neem tree were collected from CSIR-NCL campus. These leaves after proper drying process were crushed into fine powder and heated using a split tube furnace in an inert atmosphere at 1000 °C for 4 h. The obtained black product was then subjected to ball milling to obtain fine porous carbon powder, which is now termed as leaves derived carbon (LDC) [41].

2.5 Characterizations

In this paper we focus mainly on the use of three porous carbons (HPGN, PDG and LDC) as cathode materials for highly efficient advanced Li-HEC application. Therefore, in the characterization section we have mainly emphasized the properties as revealed by the electrochemistry techniques used for the Li-HEC study along with some added physical characterizations such as thermogravimetric analysis (TGA in N_2 gas atmosphere) and X-ray photo electron spectroscopy (XPS, by using ESCA-3000, VG Scientific Ltd. to analyse surface functionality). All the rest characterizations of the powdered samples by different physical techniques such as X-ray diffraction, Raman analysis, BET surface area analysis, morphological studies by using high resolution transmission electron microscopy (HR-TEM) and field emission scanning electron microscopy (FE-SEM) for all the three materials have been fully discussed in our previous reports [39-41]. The key techniques like XRD and Raman were applied to all the three porous carbon materials and the data are presented in the Electronic Supplementary Information (ESI, Figure S1 a, b). In order to reveal the porous structures in the three carbons

under study only HRTEM images are presented in the (electronic supporting information (Please see ESI, Figure S2).

2.6 Electrochemical measurements

All the electrochemical measurements were carried out by the standard two electrodes CR 2016 coin cell assembly. The composite test electrodes were formulated with 80% active material, 10% of conducting carbon (Super-P), 10% of binder (teflonized acetylene black, TAB-2) with ethanol as a solvent and pressed over 200 mm^2 stainless steel mesh (Goodfellow, UK). For the single electrode performance (half-cells), insertion type material $Li_4Ti_5O_{12}$, HPGN, PDG, LDC and commercial AC were used as working electrode and metallic lithium served as both counter and reference electrode. Microporous fiber (Whatman, Cat. No. 1825-047, UK) was used as a separator and filled with 1M $LiPF_6$ in ethylene carbonate (EC)/dimethyl carbonate (DMC) (1:1 wt.%, Selectipur LP 30, Merck KGaA, Germany) as electrolyte solution for both half-cell and Li-HEC assembly.

3. Results and Discussion

The as synthesized HPGN, PDG, and LDC were characterised by using TGA technique. Figure 1 shows the TGA data of all these carbonaceous materials in N_2 gas atmosphere. More weight loss for HPGN (38%) suggests higher population of oxygen containing functionalities therein than PDG (29%) and LDC (23%) samples. For comparison the CAC TGA plot has also been included in Figure 1 It is well known that, reduced graphene oxide (chemically prepared material by reduction of GO at ~ 100 °C) always contains some unreduced oxygen containing function groups [43, 44]. Therefore, the HPGN sample clearly contains more percentage of oxygen

functionalities than PDG and LDC which were synthesized at 1000° C. The higher content for oxygen containing functionalities in HPGN powder is further confirmed by XPS spectroscopy. The C 1s plots for three cases (HPGN, PDG and LDC) are shown in Figure S3 (a-c) (ESI). Along with the main graphitic peak (C=C) located at 284.5 eV other possible linkages between C and O are deconvoluted in each case. As expected the number of functional groups (oxygen containing functionalities) is found to more for HPGN (~16 %) than other two PDG (~5.4 %) and LDC (12 %) [Please see Table S1]. The trend is similar to the TGA results. Such heteroatom containing groups are very important to improve the capacitive charge storage. We also plotted the O 1s plots for the three samples (please see Figure S3 d-f). Clearly the peak is broader supporting higher functionalities in HPGN sample than other two cases. The O1s results are similar to the C1s results. We also used Raman spectroscopy to explain the more pronounced and beneficial structural change (morphology modification) in HPGN sample useful for charge-storage (Please see Figure S1 b-c). The G-line in Raman spectrum is primarily due to >C=C< group that is expected equally in all three cases (~1600 cm^{-1}). However we mainly focused on D-band nature of HPGN, PDG and LDC sample. The D line for HPGN sample (please see plot S1 b) is broader and more intense due to numerous oxygen containing groups on the surface of HPGN and hierarchical porosity (1-140 Aº). Sharp edges within the perforated network of HPGN are mainly responsible to broaden the D line than that of PDG and LDC. Overall, the hierarchical porosity (1-140 Aº) and number of active edge sites supports the enhanced course of charge storage for HPGN than PDG and LDC samples. (Please see electrochemical performance section).

The capacitive behaviour of the carbonaceous material tested above the open circuit voltage (OCV) (*vs.* Li) is ascribed to the reversible adsorption and desorption behaviour of anions present in the electrolyte (PF_6^-) and subsequent electric double layer formation across the electrode/electrolyte interface [14, 15, 21, 24, 28]. Further, such single electrode performance is very crucial to balance the mass between the electrodes during the fabrication of Li-HEC. Usually, in conventional symmetric supercapacitor the applied potential is equally distributed to the electrodes. However, in the asymmetric configuration, particularly Li-HEC the two electrodes undergo different energy storage mechanisms hence the applied potential is split into specific capacitance of the individual electrodes. This un-equal distribution leads to the partial utilization of the electro-active material, as a result suppression of energy density [21, 28]. Therefore the mass balance between the electrodes is mandatory to realize complete utilization of the active material and subsequently to develop high energy density Li-HEC. Therefore, half-cells were constructed and tested from OCV to the decomposition potential of conventional carbonate based electrolyte (3–4.6 V *vs*. Li) and the data are shown in Figure 2.

Figure 2a shows the typical galvanostatic charge-discharge curves at a current density of 100 mA g^{-1}. Irrespective of the carbonaceous materials, all the four electrodes displayed linear variation of potential with respect to time. Such linear variation corresponds to the perfect reversible adsorption/desorption of PF_6^- anions [15, 21]. Amongst these the HPGN showed the highest reversible capacity of ~69 mAh g^{-1} as compared to PDG (38 mAh g^{-1}), LDC (32 mAh g^{-1}) and CAC (33 mAh g^{-1}) electrodes. The observed values for the HPGN are almost two times higher than the rest of the counterparts as evidently seen from Figure 2a. Further, because of the higher electrochemical performance of HPGN in single electrode configuration, a small amount

of its loading was required in full cell (vs. $Li_4Ti_5O_{12}$), which certainly prohibits the suppression of volumetric density. The main reason for the high capacity value of perforated graphene is due to the perfect and high degree of graphitization of this material, which provides strong adsorption/de-sorption behaviour against PF_6^- anions. We mention the terms perfect and high degree of graphitization for HPGN because it is prepared by reduction of hierarchically perforated graphite oxide (HPGO) which has originally been obtained from graphite powder. Therefore after reduction, the disturbed graphitic structure of HPGO is perfectly regained in HPGN. In contrast, the lack of formation of perfect graphitic structure in other forms (PDG and LDC) leads to poorer performance than HPGN although they also exhibit high surface area and porosity. Interestingly, the observed values for the polymer derived graphene (PDG) and bio-mass/leaf derived (LDC) carbons delivered more or less the same reversible capacity as compared to the CAC. The reason behind this is less degree of graphitization in PDG and LDC samples due to usage of non-graphitic precursor source. For example, PDG involves use of polymer (Poly (4-styrene sulfonic acid-co-maleic acid) sodium salt) and LDC is obtained from dead leaves. Hence, in these two samples (PDG and LDC) the degree of graphitization is achieved by pyrolysis of respective non graphitic precursors whereas in HPGN it is regained after HPGO reduction. Therefore, the obtained capacities in the case of PDG (38 mAh g^{-1}) and LDC (32 mAh g^{-1}) are smaller than HPGN (69 mAh g^{-1}) due to less degree of graphitization (turbostatic). Similar kind of Li-adsorption/de-sorption properties is noted for such graphene nanosheets while testing as anode material for Li-ion battery applications. The reversible capacity can be converted into the specific capacitances (C_{SP}) by using the following equation proposed by Amatucci *et al.* [15].

$$C_{SP}\ (F\,g^{-1}) = \frac{i\,(A)\times t\,(s)}{3600\times m\,(g)} = mAh\,g^{-1}(\text{observed capacity})\times\frac{3600}{dV(mV)}$$

where, *i* is applied current, *t* is discharge time, *m* weight of the active material and *dV* is testing window of the aforementioned half-cell configuration (1600 mV). However, the said relation is valid if the variation of voltage with respect to time is linear. By employing the above equation specific capacitances of ~155, ~86, ~72 and ~74 F g^{-1} are noted for HPGN, PDG, LDC and CAC, respectively. Plot of the specific discharge capacitance *vs.* cycle number is given in Figure 2b. All the electrodes exhibit a very stable cycling profile except for a slight fading in the initial cycles. Capacitance fading in initial cycles is common for the case of non-aqueous electrolytes [12]. Even after 1000 cycles very less fading in the specific capacitances is noticed for each of the three samples, which is quite significant in non-aqueous medium. Thus, from the results it is now important to emphasize on the performance of HPGN, which is far better than the conventionally employed AC. Based on the electrochemical performance of the spinel phase $Li_4Ti_5O_{12}$ under the same current rate (Figure S4 ESI), the active material loading of anode ($Li_4Ti_5O_{12}$) to carbonaceous cathodes is optimized into 1:2.47, 1:4.44, 1:5.26 and 1:5.15 for HPGN, PDG, LDC and CAC, respectively, during the fabrication of Li-HEC.

Li-HEC was constructed using carbonaceous cathode and insertion type spinel phase $Li_4Ti_5O_{12}$ anode and cycled over 1-3 V testing range at various current densities under the optimized mass loadings described above and the results are shown in Figure 3 (a-c). The corresponding cycling data for CAC/ $Li_4Ti_5O_{12}$ is shown in Figure S5. All the Li-HEC showed a very small ohmic drop ~3 V followed by monotonous discharge curves and a sudden drop of potential (~1.4 V onwards). Monotonous discharge curves correspond to the breaking of the electric double layer across electrode/electrolyte interface and simultaneous extraction of Li-

from the spinel lattice. Once all the Li has been extracted, the cell undergoes a sudden drop, which has been clearly evidenced for all the cases. The Li-HEC comprising HPGN cathode showed prolonged discharge time irrespective of the applied current densities compared to the rest of the cells (Figure 3a). The extended discharge time of HPGN is consistent with the single electrode performance noted above. Specific energy (E_{SP}) and power densities (P_{SP}) of the Li-HEC are calculated using the following relation,

$$P_{sp} = {}^{\Delta E \,.\, i}/_{M} \text{ and } E_{sp} = \left(P_{sp} \,.\, t\right)$$

where, $\Delta E = (E_{max} + E_{min})/2$ and E_{max} and E_{min} are respectively the potential at beginning of discharge and at the end of discharge curves of galvanostatic cycle and *M* active mass loading of both electrodes (mg, anode + cathode) [21, 24, 27, 28]. The Li-HEC delivered the maximum energy density of ~65, ~42, ~35 and ~36 Wh kg^{-1} for HPGN, PDG, LDC and CAC cathodes, respectively at corresponding power density of 0.5 kW kg^{-1} (Ragone Plot figure 3 d). Moreover, the observed energy density is one of the best values other than pre-lithiated graphite anode, for example Stoller *et al.*[38] reported the performance of Li-HEC comprising a-MEGO cathode and $Li_4Ti_5O_{12}$ anode delivering a maximum energy density of 40.8 Wh kg^{-1}. The enhanced energy density because of the graphitic nature of nanosheets with appreciable amount of porosity, allows easy access to the electrolyte solution and thereby enables strong adsorption/de-sorption behaviour of anions present in the solution [3, 5].

In all samples under study the presence of porosity is beneficial for achieving high specific capacitance and hence energy density. The BET surface area of HPGN is found to be 260 m^2/g, which is much lower than PDG (1720 m^2/g) [40] and LDC (1230 m^2/g) [41]. Even

though the surface area is less for HPGN, the efficient performance is attributed to presence of accentuated electric field [39] at each wall of nano-perforations, which is absent in the PDG, LDC and CAC samples. Comparison of pore size distribution for all the three materials is shown in figure S6 (ESI). The distribution of pores explains the achieved higher electrochemical performance of HPGN as compared to LDC and PDG. It is a well established fact that, carbon-based materials possessing meso and microporosity with optimum surface area lead to better supercapacitor performance than the material having only microporosity and higher surface area. The presence of mesopores accelerates the diffusion process of electrolyte ions. This allows usage of maximum area for adsorption and thereby increases the capacitance [45]. For instance, the supercapacitor properties of coconut shell derived carbon [45] are significantly superior than the MOF derived carbon [46] although the latter possesses greater surface area (~2714 $m^2 g^{-1}$) than coconut shell derived carbon (~1652 $m^2 g^{-1}$). The main reason is attributed to the presence of a balanced combination of micro and mesopores in coconut shell derived carbon as compared to that in the case of MOF derived carbon which primarily contains micropores.

These important observations helped us to elaborate the best performance of HPGN over LDC and PDG samples. Out of the three samples, LDC and PDG exhibit high surface area with bi-modal pore size distribution in the micropore region whereas HPGN shows hierarchical pore size distribution in micro as well as mesopores region. Thus, it can be concluded that the presence of mesopores in HPGN is an additional advantage to accumulate maximum PF_6^- ions thereby rendering a higher capacitance value than LDC and PDG. We also plotted the cumulative pore volume plots for three samples and results are presented as figure S7. Due to hierarchical porosity (from 1-140 Aº) the pore volume for HPGN is found to be lesser (0.42 $cm^3 g^{-1}$) than PDG (2.49 $cm^3 g^{-1}$) and LDC (0.82 $cm^3 g^{-1}$) samples. Though the pore volume is less

the number of sharp edges due to hierarchical porosity is high thereby increasing the course of charge storage. We again re-highlight the importance of such hierarchical porosity in HPGN sample over other two samples (PDG and LDC). Such specific consideration previously reported by us [39] clearly supports the superior performance of HPGN than PDG and LDC samples.

Moreover, as revealed from TGA the weight loss for HPGN (~38%) is more than LDC (29%) and PDG (23%). This indicates the presence of some non-reduced oxygen functionalities in HPGN. Recently, Lee *et. al.* [47] studied the importance of hetero-atom functionality (Amide) in urea reduced graphene oxide (URGO) for efficient Li-HEC cathode. These authors highlighted the importance of functional groups and Li^+ ions interaction for the increased capacity. Mhamane *et al.* reported use of trigol reduced graphene (TRG) containing oxygen functionalities as efficient Li-HEC cathode [48]. In addition to TGA similar observation has been confirmed by XPS plots (Figure S3).Therefore, we believe that the functionalities present on HPGN are also responsible for the observed superior Li-HEC properties. In summary, the three advantages of HPGN namely the presence of accentuated electric field at each wall of nano-perforations, balanced micro as well as mesoporosity, and the presence of oxygen containing functionalities are together responsible for its superior performance over PDG, LDC and CAC. No big differences in the energy densities of Li-HEC containing PDG, LDC and CAC cathodes at low current rates are noted except the power capabilities. The enhanced energy and power density of the HPGN comprising Li-HEC has the promise to power the HEV and EV.

Cycleability is another important criterion to employ them in aforementioned high power applications. Among the carbonaceous materials investigated, HPGN is found to be superior also in terms of both the high energy and power density in the Li-HEC assembly. In this line, long

term cycleability was conducted to ensure the performance. The Li-HEC comprising HPGN cathode and $Li_4Ti_5O_{12}$ anode was cycled at constant current density of 2 A g^{-1}. The observed values are normalized and presented in Figure 4. A marginal increase in the capacity profiles during cycling is noted which is probably due to the slower participation of the active material in the electrochemical reaction. After 1500 cycles, the Li-HEC retains ~92% of initial value. The small fading is mainly due to the intrinsic nature of the commercially available insertion type electrode $Li_4Ti_5O_{12}$. Further capacity fading during cycling of such electrode in a single electrode configuration is clearly evidenced from Figure S4. Nevertheless, this fading issue can be definitely eased by adopting highly conducting networks such as CNT or carbon nanofibers as suggested by Naoi and co-workers [12, 16-19]. The present result clearly shows that an appropriate tailoring of graphene nanosheets (*i.e.* perforation) can certainly yield a high energy density electrochemical energy storage device.

4. Conclusions

High energy density Li-ion hybrid electrochemical capacitors were fabricated by differently synthesized forms of high surface area conducting carbons. The Li-HEC made using hierarchically perforated graphene nanosheets (HPGN) as cathode and commercial spinel phase as $Li_4Ti_5O_{12}$ anode in non-aqueous medium was found to be the best. It delivered maximum energy density of ~65 Wh kg^{-1} and corresponding power density 0.5 kW kg^{-1} for 100% depth of discharge. The Li-HEC comprising HPGN also rendered excellent cycleability and was shown to retain ~99.5% initial capacitance after 1000 cycles. Such exceptional performance can be mainly to the high conductance graphitized structure with appropriate porosity. This result paves the way for the development of high energy density Li-HEC power packs.

Acknowledgements

SBO acknowledge support under CSIR-TAPSUN program. AS thanks UGC for fellowship support. VA and SM thank the National Research Foundation (NRF, Singapore) for financial support through the Competitive Research Programme (CRP) (Grant no. NRF-CRP4-2008-03).

References

[1] N.-S. Choi, Z. Chen, S.A. Freunberger, X. Ji, Y.-K. Sun, K. Amine, G. Yushin, L.F. Nazar, J. Cho, P.G. Bruce, Challenges Facing Lithium Batteries and Electrical Double-Layer Capacitors, Angew.Chem. Int. Ed., 51 (2012) 9994 - 10024.

[2] P. Simon, Y. Gogotsi, Materials for electrochemical capacitors, Nat. Mater., **7**(2008) 845 - 854.

[3] M.Inagaki, H. Konno, O. Tanaike, Carbon materials for electrochemical capacitors, J. Power Sources, 195 (2010) 7880 - 7903.

[4] E.J. Cairns, P. Albertus, Batteries for electric and hybrid-electric vehicles, Annu. Rev.Chem. Biomol. Eng., 1 (2010) 299-320.

[5] E. Frackowiak, F. Béguin,Carbon materials for the electrochemical storage of energy in capacitors, Carbon, 39 (2001) 937-950.

[6] V.V.N. Obreja, On the performance of supercapacitors with electrodes based on carbon nanotubes and carbon activated material—A review, Physica E: Low-dimensional Systems and Nanostructures, 40 (2008) 2596- 2605.

[7] D.S. Su, R. Schlögl, Nanostructured Carbon and Carbon Nanocomposites for Electrochemical Energy Storage Applications, ChemSusChem, 3 (2010) 136-168.

[8] K. Karthikeyan, S. Amaresh, V. Aravindan, Y.S. Lee, Microwave assisted green synthesis of MgO–carbon nanotube composites as electrode material for high power and energy density supercapacitors, J. Mater. Chem. A, 1 (2013) 4105 - 4111.

[9] L.L. Zhang, R. Zhou, X.S. Zhao, Graphene-based materials as supercapacitor electrodes, J. Mater. Chem., 20 (2010) 5983 - 5992.

[10] Y. Huang, J. Liang, Y. Chen, An Overview of the Applications of Graphene-Based Materials in Supercapacitors, Small, 8 (2012) 1805 - 1834.

[11] K. Naoi, P. Simon, New Materials and New Configurations for Advanced Electrochemical Capacitors, Electrochem. Soc. Interface, 17 (2008) 34-37.

[12] K. Naoi, Y. Nagano, Li-Ion-Based Hybrid Supercapacitors in Organic Medium, in: Supercapacitors, Wiley-VCH Verlag GmbH & Co. KGaA, 239 (2013).

[13] V. Aravindan, J. Gnanaraj, Y.-S. Lee, S. Madhavi, $LiMnPO_4$ – A next generation cathode material for lithium-ion batteries, J. Mater. Chem. A, 1 (2013) 3518 - 3539.

[14] I. Plitz, A. DuPasquier, F. Badway, J. Gural, N. Pereira, A. Gmitter, G.G. Amatucci, The design of alternative nonaqueous high power chemistries, Appl. Phys. A: Mater. Sci.Process., 82 (2006) 615-626.

[15] G.G. Amatucci, F. Badway, A. Du Pasquier, T. Zheng, An Asymmetric Hybrid Nonaqueous Energy Storage Cell, J. Electrochem. Soc., 148 (2001), A930-A939.

[16] K. Naoi, Nanohybrid Capacitor': The Next Generation Electrochemical Capacitors, Fuel Cells, 10 (2010) 825-833.

[17] K. Naoi, S. Ishimoto, Y. Isobe, S. Aoyagi, High-rate nano-crystalline $Li_4Ti_5O_{12}$ attached on carbon nano-fibers for hybrid supercapacitors, J. Power Sources, 195 (2010) 6250- 6254.

[18] K. Naoi, S. Ishimoto, J.-i. Miyamoto, W. Naoi, Second generation 'nanohybrid supercapacitor': Evolution of capacitive energy storage devices, Energy Environ. Sci., 5 (2012) 9363- 9373.

[19] K. Naoi, W. Naoi, S. Aoyagi, J.-i. Miyamoto, T. Kamino, New generation "nanohybrid supercapacitor", Acc. Chem. Res., 46 (2013) 1075- 1083.

[20] C.V. Rao, B. Rambabu, Nanocrystalline $LiCrTiO_4$ as anode for asymmetric hybrid supercapacitor, Solid State Ionics, 181 (2010) 839 - 843.

[21] V. Aravindan, W. Chuiling, S. Madhavi, High power lithium-ion hybrid electrochemical capacitors using spinel $LiCrTiO_4$ as insertion electrode, J. Mater. Chem., 22 (2012) 16026-16031.

[22] V. Aravindan, M.V. Reddy, S. Madhavi, G.V.S. Rao, B.V.R. Chowdari, Electrochemical Performance of α-MnO_2 Nanorods/Activated Carbon Hybrid Supercapacitor, Nanosci. Nanotechnol. Lett, 4 (2012) 724-728.

[23] C. Xu, F. Kang, B. Li, H. Du, Recent Progress on Manganese Dioxide Based Supercapacitors, J Mater Res, 25 (2012) 1421-1432.

[24] V. Aravindan, N. Shubha, W.C. Ling, S. Madhavi, Constructing high energy density non-aqueous Li-ion capacitors using monoclinic TiO_2-B nanorods as insertion host, J. Mater. Chem. A, 1 (2013) 6145-6551.

[25] Q. Wang, Z.H. Wen, J.H. Li, A Hybrid Supercapacitor Fabricated with a Carbon Nanotube Cathode and a TiO_2–B Nanowire Anode, Adv. Funct. Mater., 16 (2006) 2141- 2146.

[26] L. Cheng, H.Q. Li, Y.Y. Xia, A hybrid nonaqueous electrochemical supercapacitor using nano-sized iron oxyhydroxide and activated carbon, J. Solid State Electrochem., 10 (2006) 405 - 410.

[27] V. Aravindan, M.V. Reddy, S. Madhavi, S.G. Mhaisalkar, G.V. Subba Rao, B.V.R. Chowdari, Hybrid supercapacitor with nano-TiP_2O_7 as intercalation electrode, J. Power Sources, 196 (2011) 8850 - 8854.

[28] V. Aravindan, W. Chuiling, M.V. Reddy, G.V.S. Rao, B.V.R. Chowdari, S. Madhavi, Carbon coated nano-$LiTi_2(PO_4)_3$ electrodes for non-aqueous hybrid supercapacitors, Phys Chem Chem Phys, 14 (2012) 5808-5814.

[29] K. Karthikeyan, V. Aravindan, S. Lee, I. Jang, H. Lim, G. Park, M. Yoshio, Y. Lee, Electrochemical performance of carbon-coated lithium manganese silicate for asymmetric hybrid supercapacitors, J. Power Sources, 195 (2010) 3761-3764.

[30] K. Karthikeyan, V. Aravindan, S. Lee, I. Jang, H. Lim, G. Park, M. Yoshio, Y. Lee, A novel asymmetric hybrid supercapacitor based on Li_2FeSiO_4 and activated carbon electrodes, J. of Alloys Compd., 504 (2010) 224-228.

[31] X.-L. Wu, L.-Y. Jiang, F.-F. Cao, Y.-G. Guo, L.-J. Wan, $LiFePO_4$ nanoparticles embedded in a nanoporous carbon matrix: Superior cathode material for electrochemical energy-storage devices, Adv. Mater., 21 (2009) 2710-2714.

[32] R. Vasanthi, D. Kalpana, N.G. Renganathan, Olivine-type nanoparticle for hybrid supercapacitors, J. Solid State Electrochem., 12 (2008) 961-969.

[33] H. Wu, C.V. Rao, B. Rambabu, Electrochemical performance of $LiNi_{0.5}Mn_{1.5}O_4$ prepared by improved solid state method as cathode in hybrid supercapacitor, Mater Chem Phys, 116 (2009) 532-535.

[34] V. Aravindan, Y.L. Cheah, W.F. Mak, G. Wee, B.V.R. Chowdari, S. Madhavi, Fabrication of High Energy-Density Hybrid Supercapacitors Using Electrospun V_2O_5 Nanofibers with a Self-Supported Carbon Nanotube Network, ChemPlusChem, **77 (**2012) 570-575.

[35] K. Karthikeyan, S. Amaresh, K.J. Kim, S.H. Kim, K.Y. Chung, B.W. Cho, Y.S. Lee, A high performance hybrid capacitor with Li_2CoPO_4F cathode and activated carbon anode, Nanoscale, 5 (2013) 5958-5964.

[36] Z. Yang, D. Choi, S. Kerisit, K.M. Rosso, D. Wang, J. Zhang, G. Graff, J. Liu, Nanostructures and lithium electrochemical reactivity of lithium titanites and titanium oxides: A review, J. Power Sources, 192 (2009) 588-598.

[37] Y. Zhu, S. Murali, W. Cai, X. Li, J.W. Suk, J.R. Potts, R.S. Ruoff, Graphene and graphene oxide: synthesis, properties, and applications, Adv. Mater., 22 (2010) 3906-3924.

[38] M.D. Stoller, S. Murali, N. Quarles, Y. Zhu, J.R. Potts, X. Zhu, H.-W. Ha, R.S. Ruoff, Activated graphene as a cathode material for Li-ion hybrid supercapacitors, Phys Chem Chem Phys, 14 (2012) 3388- 3391.

[39] D. Mhamane, A. Suryawanshi, S.M. Unni, C. Rode, S. Kurungot, S. Ogale, Hierarchically Nanoperforated Graphene as a High Performance Electrode Material for Ultracapacitors, Small, 9 (2013) 2801-2809.

[40] P. Yadav, A. Banerjee, S. Unni, J. Jog, S. Kurungot, S. Ogale, A 3D Hexaporous Carbon Assembled from Single-Layer Graphene as High Performance Supercapacitor, ChemSusChem, 5 (2012) 2159-2164.

[41] M. Biswal, A. Banerjee, M. Deo, S. Ogale, From dead leaves to high energy density Supercapacitors, Energy Environ. Sci., 6 (2013) 1249 - 1259.

[42] D. Mhamane, S. Unni, A Suryawanshi, O. Game,C Rode, B Hannoyer, S Kurungot ,S Ogale, Trigol based reduction of graphite oxide to graphene with enhanced charge storage activity, J. Mater. Chem., 22 (2012)11140 - 11145.

[43] V. H. Pham, T. V. Cuong, T.-D. Nguyen-Phan, H. D. Pham, E. J. Kim, S. H. Hur, E. W. Shin, S. Kim and Jin Suk Chung, One-step synthesis of superior dispersion of chemically convertedgraphene in organic solvents, Chem. Commun., 46 (2010) 4375- 4377.

[44] C. K. Chua and M. Pumera, Chemical reduction of graphene oxide: a synthetic chemistry viewpoint, Chem.Soc.Rev., 43 (2014) 291-312.

[45] A. Jain, V. Aravindan, S. Jayaraman, P. S. Kumar, R. Balasubramanian, S. Ramakrishna, S. Madhavi and M. P. Srinivasan, Scientific Reports, 3 (2013) 3002.

[46] A. Banerjee, K. K. Upadhyay, D. Puthusseri, V. Aravindan, S. Madhavi and S. Ogale, MOF-derived crumpled-sheet-assembled perforated carbon cuboids as highly effective cathode active materials for ultra-high energy density Li-ion hybrid electrochemical capacitors (Li-HECs), Nanoscale, 6 (2014) 4387-4394.

[47] J. H. Lee, W. H. Shin, M.-H. Ryou, J. K. Jin, J. Kim and J. W. Choi, Functionalized Graphene for High Performance Lithium Ion Capacitors, ChemSusChem, 5 (2012) 2328–2333.

[48] V. Aravindan, D. Mhamane, W. C. Ling, S. Ogale, and S. Madhavi, Nonaqueous Lithium-Ion Capacitors with High Energy Densities using Trigol-Reduced Graphene Oxide Nanosheets as Cathode-Active Material, ChemSusChem, 6 (2013) 2240–2244.

Figure Captions

Figure 1. TGA data of various carbons.

Figure 2. (a) Typical galvanostatic charge-discharge curves of various carbonaceous materials in single electrode configuration between 3-4.6 V *vs.* Li at current density of 100 mA g^{-1}, in which metallic lithium acts as counter and reference electrode. (b) Plot of specific discharge capacitance vs. cycle number. The data points are collected after every 10 cycles.

Figure 3. Galvanostatic charge-discharge profiles conducted between 1-3 V for (a) HPGN/$Li_4Ti_5O_{12}$ Li-HEC, (b) PDG/ $Li_4Ti_5O_{12}$ Li-HEC, (c) LDC/$Li_4Ti_5O_{12}$ Li-HEC and (d) Ragone plot of Li-HEC comprising various carbonaceous cathodes.

Figure 4. Plot of normalized capacitance *vs.* cycle number for HPGN/$Li_4Ti_5O_{12}$ Li-HEC at current density of 2 A g^{-1} between 1-3 V.

Figure 1

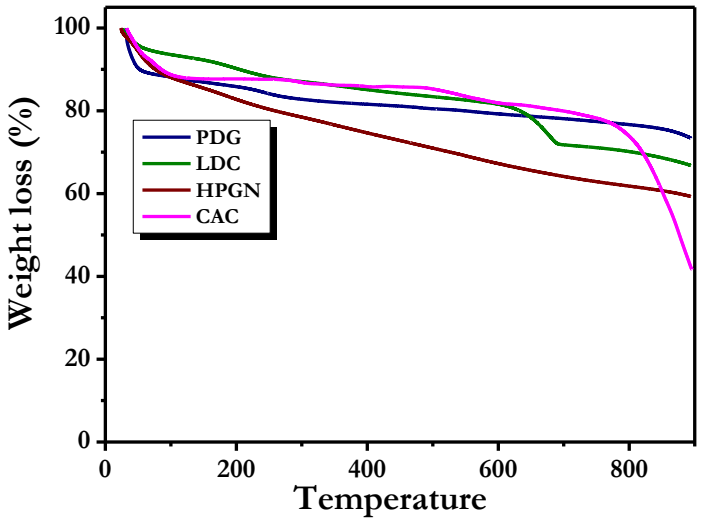
Weight loss (%)
Temperature
PDG
LDC
HPGN
CAC
0
20
40
60
80
100
0
200
400
600
800

Figure 2

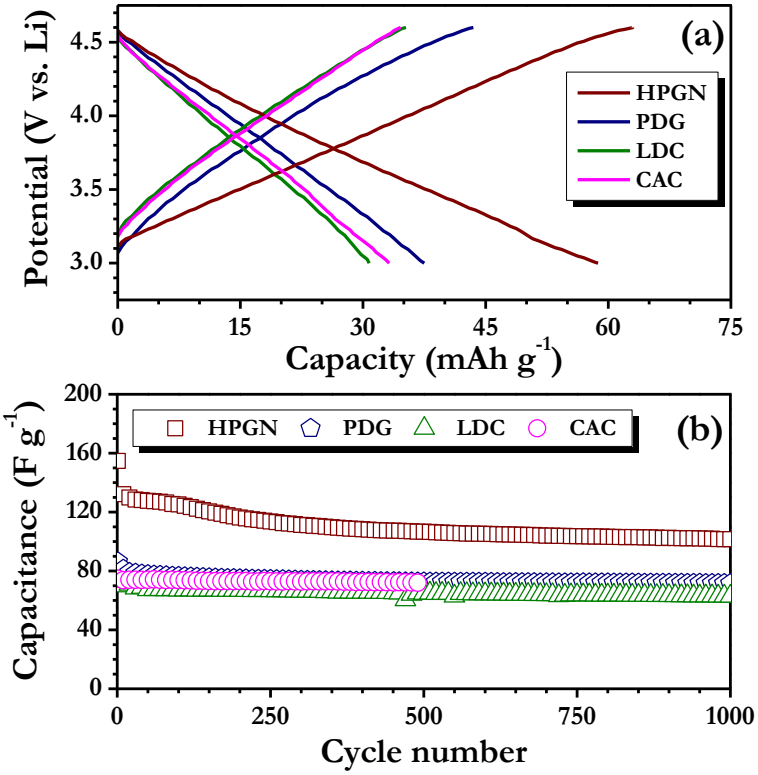
(a)
Potential (V vs. Li)
4.5
4.0
3.5
3.0
0
15
30
45
60
75
Capacity (mAh g-1)
HPGN
PDG
LDC
CAC
(b)
Capacitance (F g-1)
200
160
120
80
40
0
250
500
750
1000
Cycle number
HPGN
PDG
LDC
CAC

Figure 3

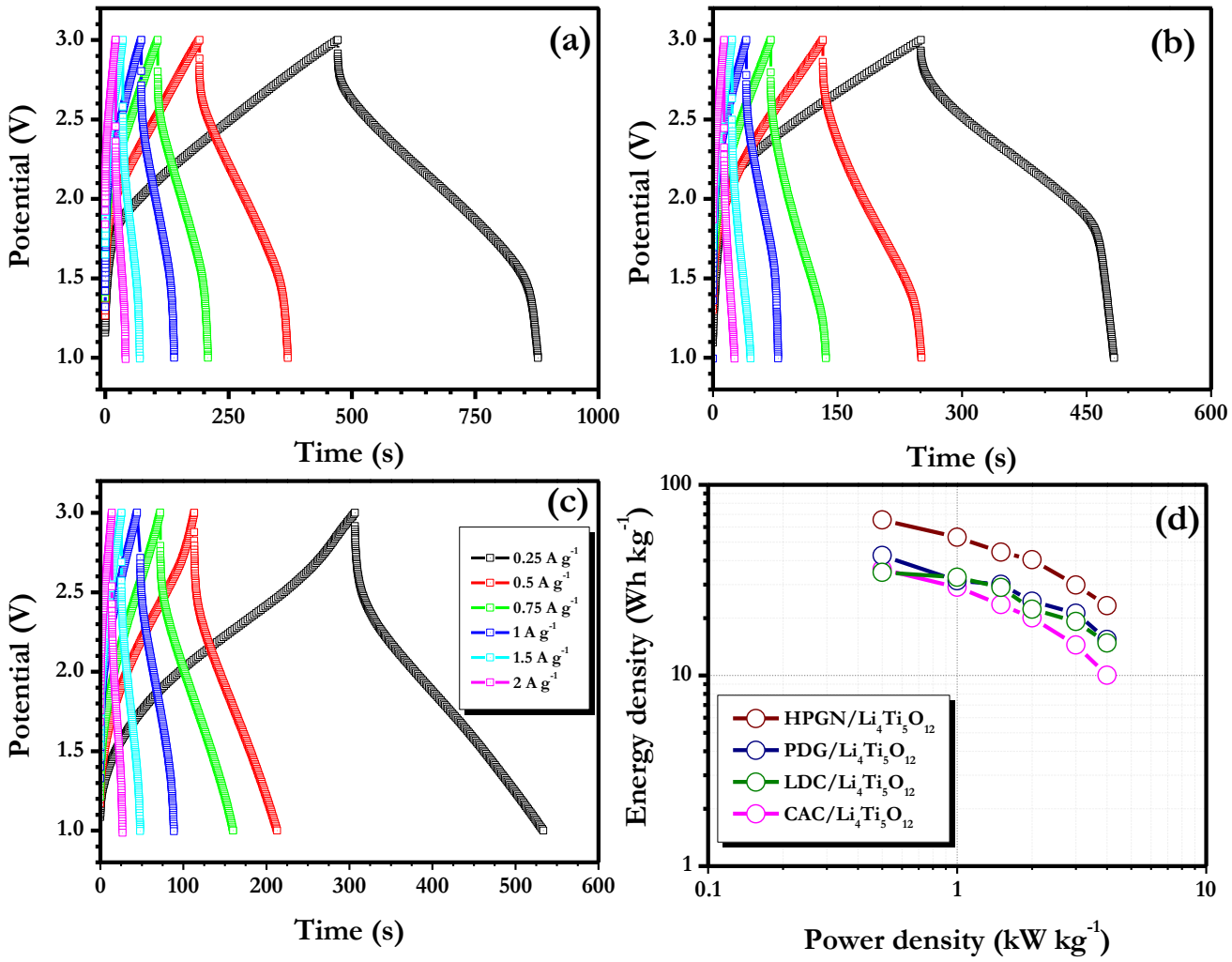
(a)
Potential (V)
Time (s)
(b)
Potential (V)
Time (s)
(c)
Potential (V)
Time (s)
0.25 A g-1
0.5 A g-1
0.75 A g-1
1 A g-1
1.5 A g-1
2 A g-1
(d)
Energy density (Wh kg-1)
Power density (kW kg-1)
HPGN/Li4Ti5O12
PDG/Li4Ti5O12
LDC/Li4Ti5O12
CAC/Li4Ti5O12

Figure 4

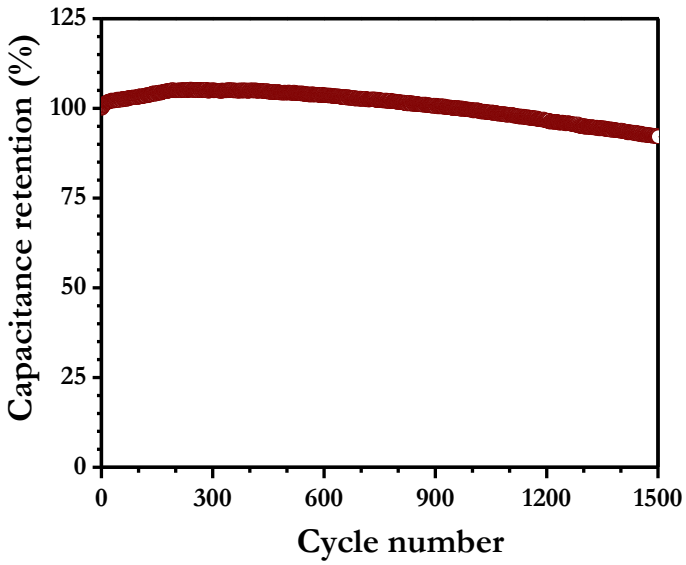
Capacitance retention (%)
125
100
75
50
25
0
0
300
600
900
1200
1500
Cycle number

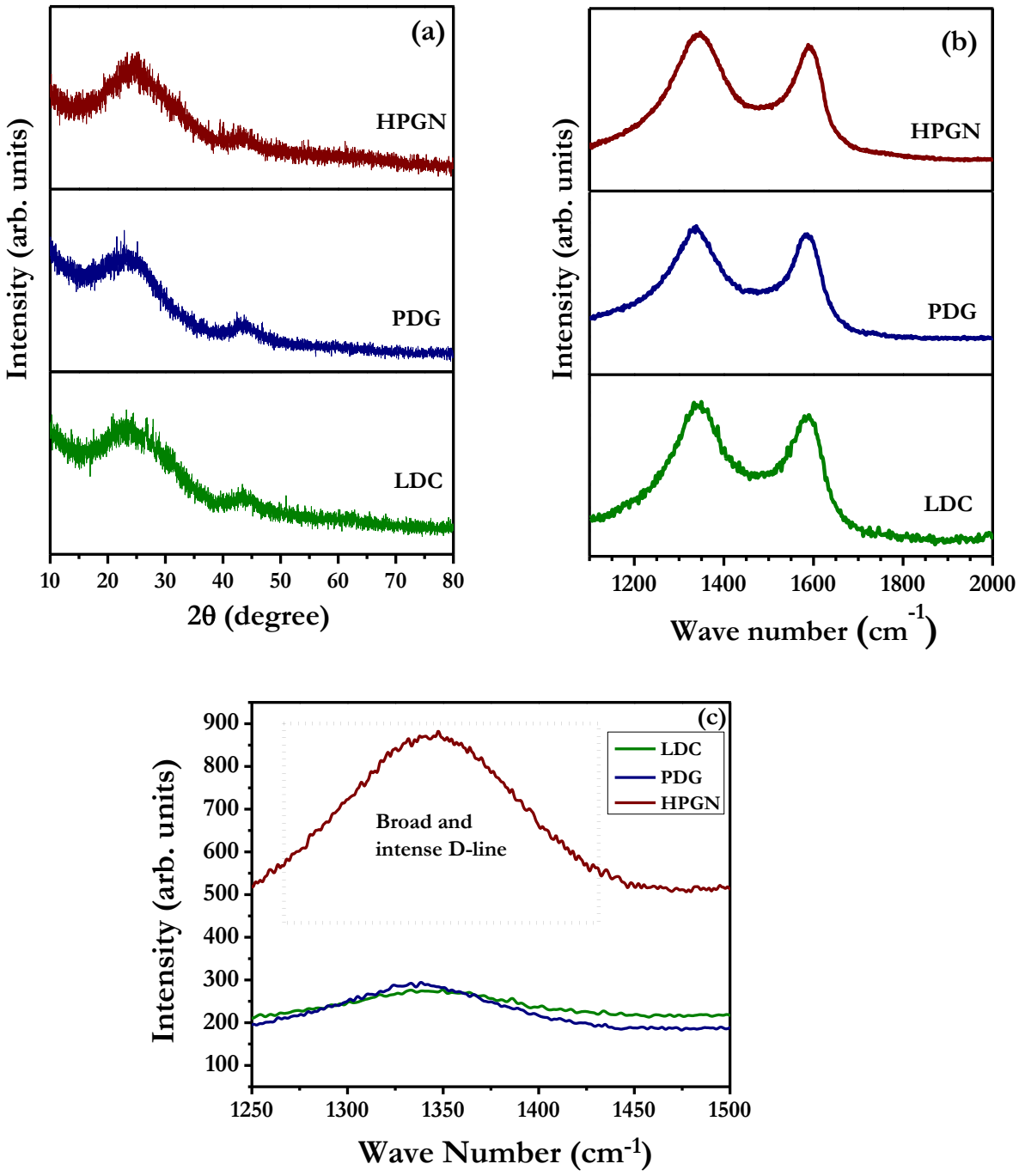

Figure S1. (a) Powder X-ray diffraction pattern, (b) Raman spectra of various carbonaceous materials obtained from different sources, and (c) Only D line Raman plot (Magnified in D line region) for HPGN, PDG and LDC samples.

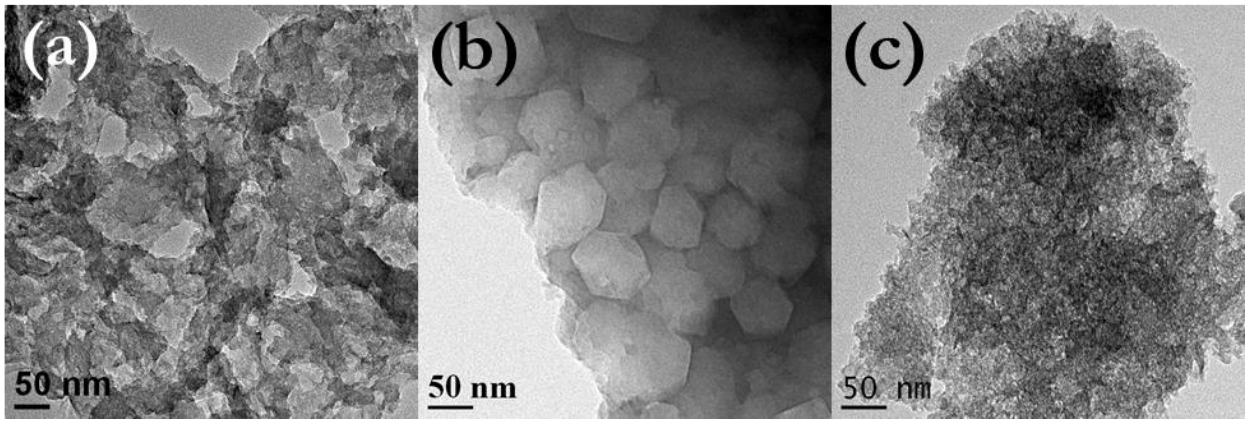

Figure S2. HR-TEM pictures of HPGN (a), PDG (b), and LDC (c).

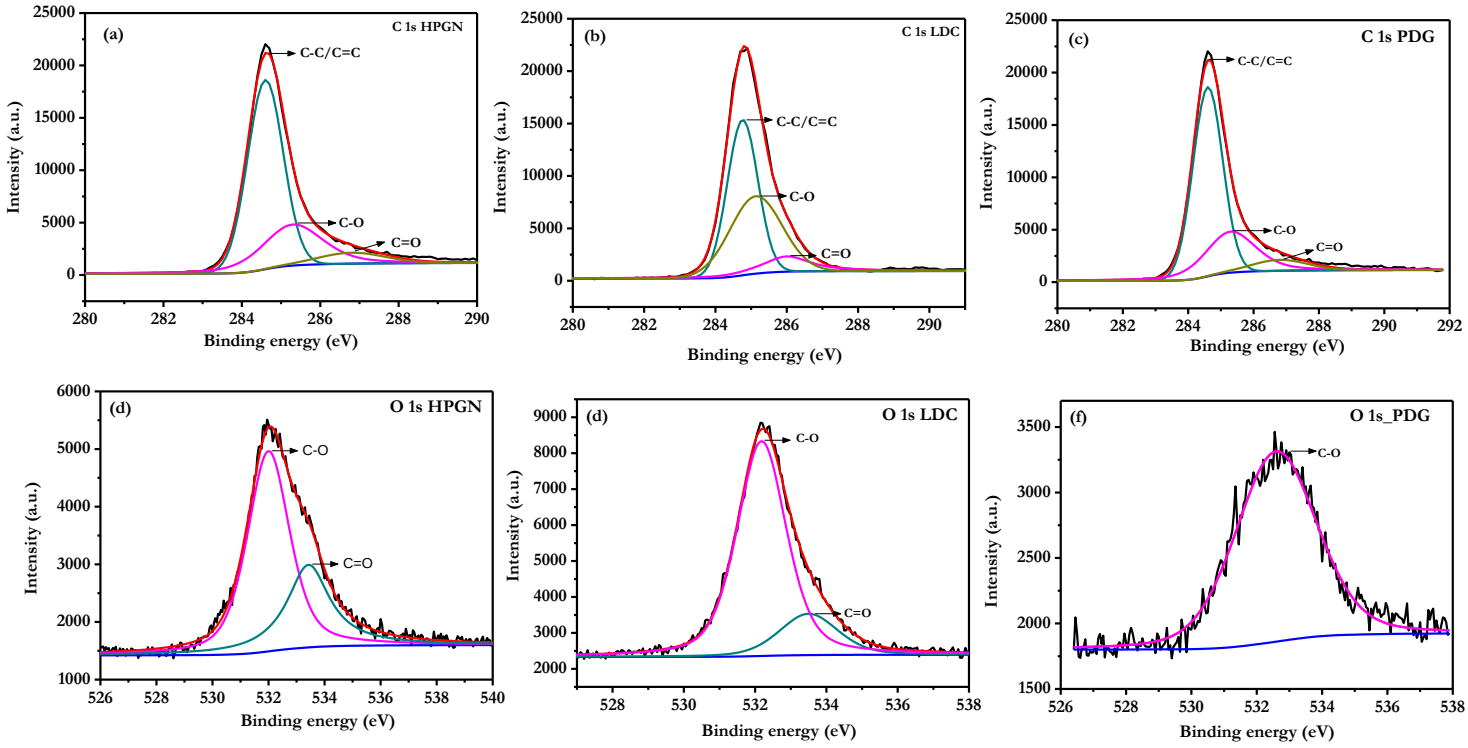

Figure S3. C 1s XPS Plots for (a) HPGN (b) LDC, (c) PDG; and O 1s plots for (d) HPGN (e), LDC, and (f) PDG samples.

Sr. No.	Sample Name	Amount of Carbon (%)	Amount of Oxygen (%)
1	**HPGN**	84.5	15.5
2	**PDG**	94.6	5.4
3	**LDC**	88	12

Table S1 XPS results comparison (C and O content) for HPGN, PDG, and LDC samples.

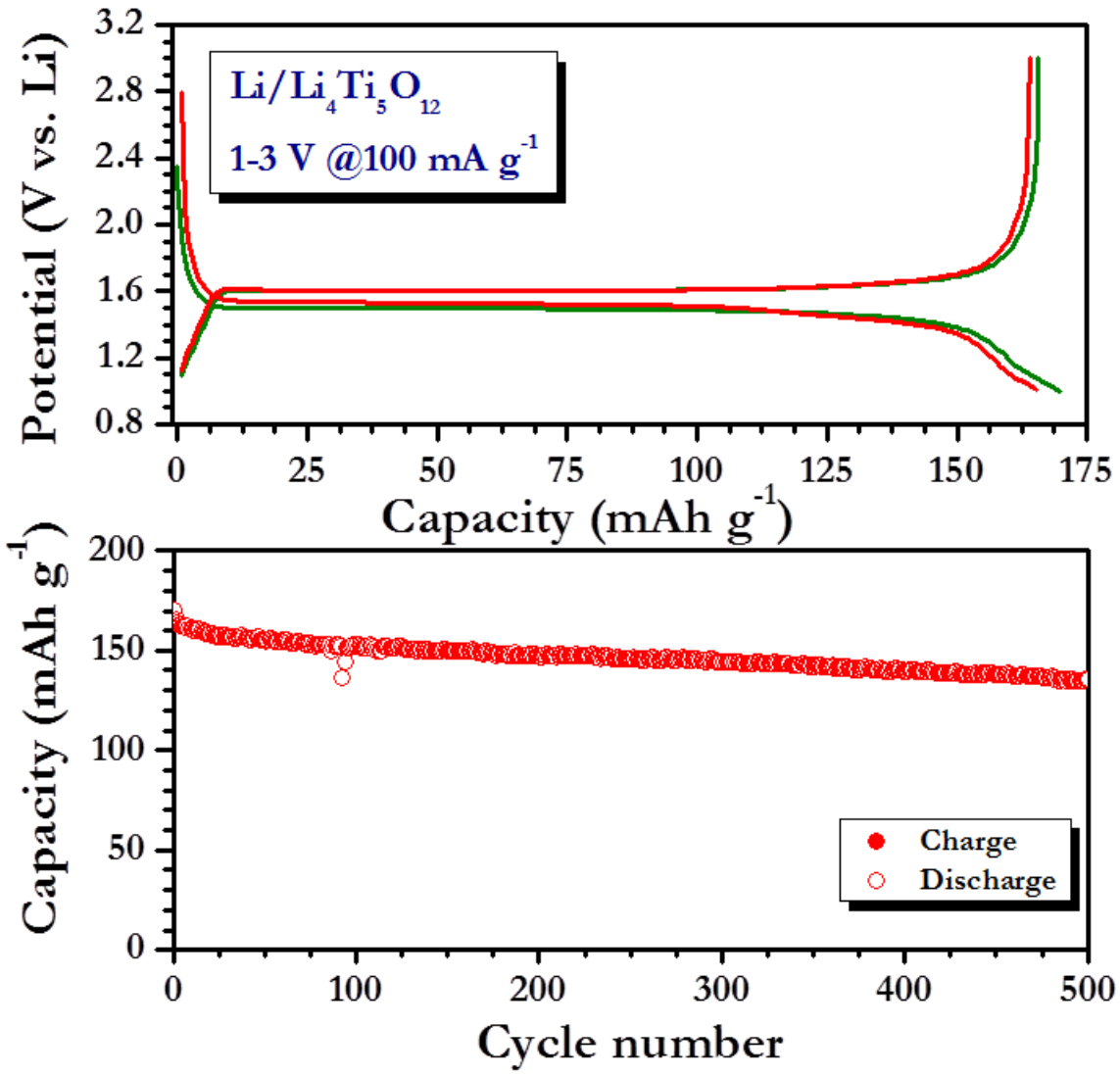

Figure S4. Galvanostatic charge-discharge curves of $Li/Li_4Ti_5O_{12}$ (Aldrich, USA) half-cells cycled between 1-3 V at constant current density of 100 mA g^{-1}, and (b) Plot of capacity *vs.* cycle number.

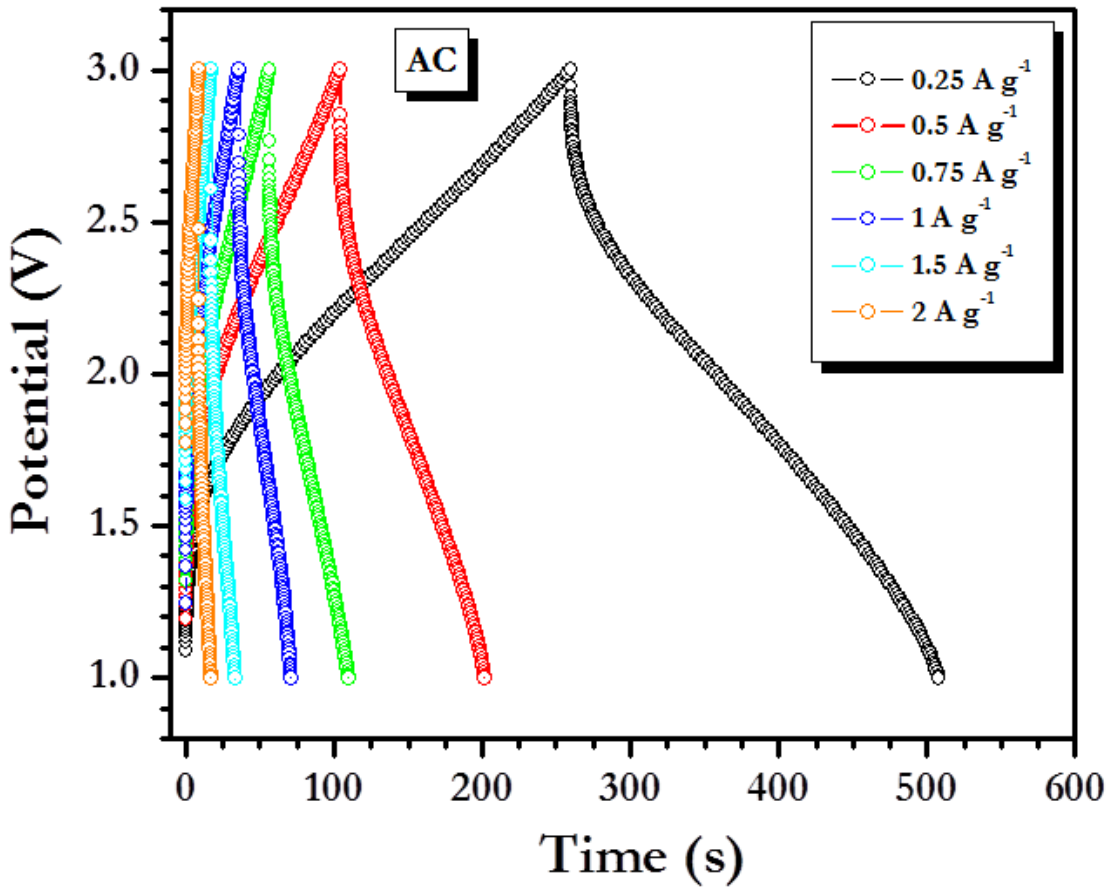

Figure S5. Galvanostatic charge-discharge profiles of commercially available activated carbon (CAC)/ $Li_4Ti_5O_{12}$ Li-HEC tested between 1-3 V.

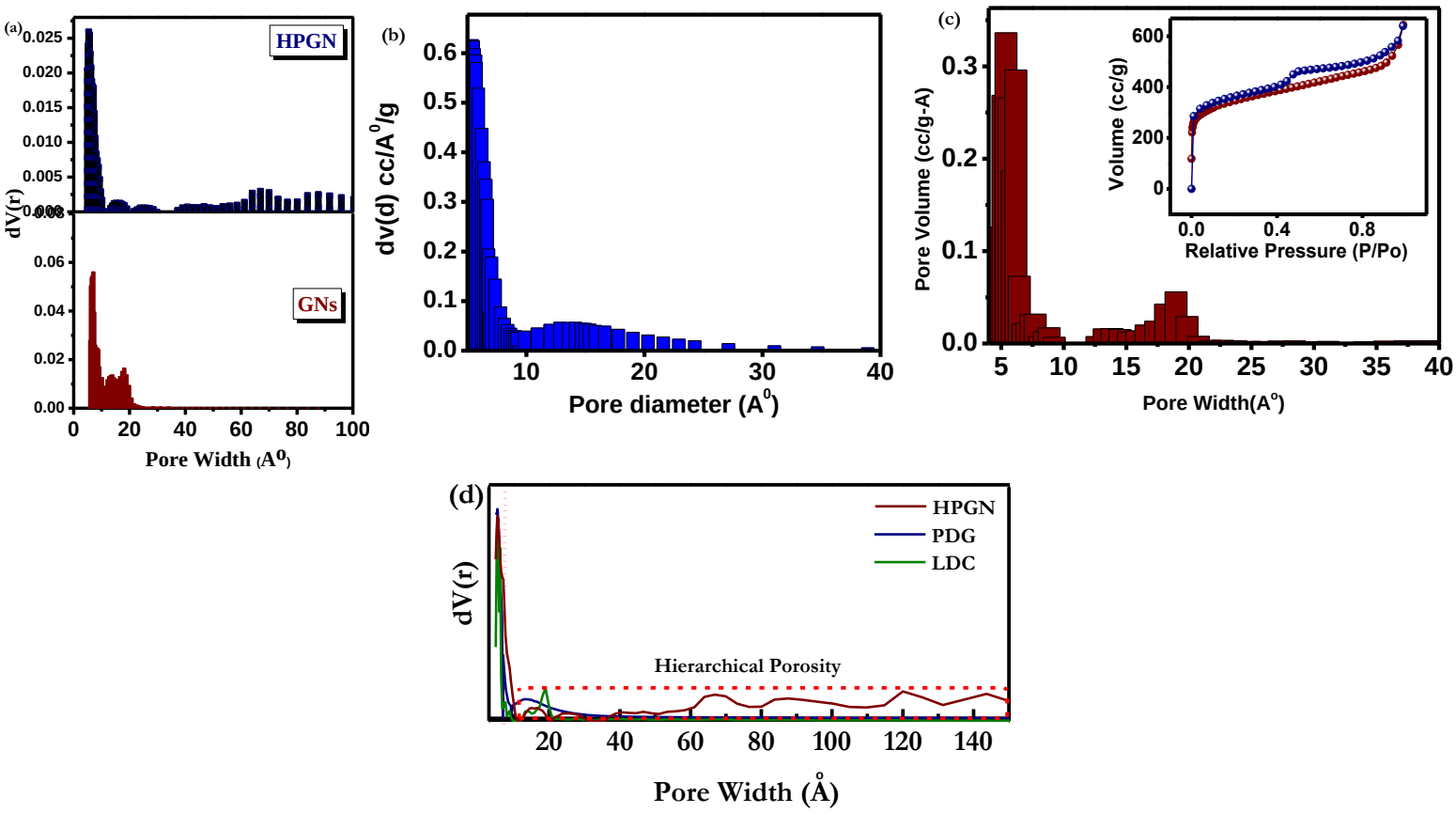

Figure S6. Pore Size distribution of (a) HPGN (b) PDG, (c) LDC reproduced with permission from [39, 40 and 41] respectively and (d) compiled pore size distribution from figures a, b, c.

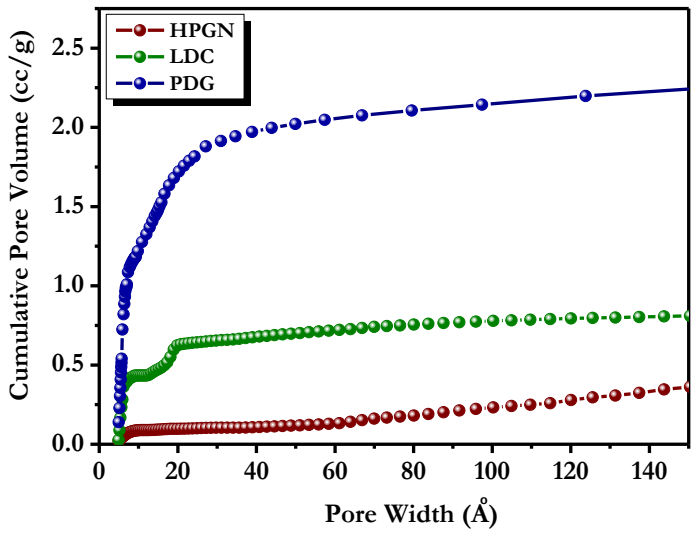

Figure S7 Cumulative pore volume plots for HPGN, PDG and LDC samples.